Vertically Emitting Microdisk Lasers

Lukas Mahler[*,1], Alessandro Tredicucci[1] and Fabio Beltram[1]
[1]NEST-INFM and Scuola Normale Superiore, Pisa
*Corresponding author: NEST-INFM, Piazza dei Cavalieri 7, I-56126 Pisa, l.mahler@sns.it

Abstract: We describe the modeling of microdisk lasers displaying vertical emission. The devices are THz quantum cascade lasers with metallic gratings fabricated along the circumference. The emission properties of the fabricated devices are well explained by the model, good mode control is obtained, and the collected power from a patterned device is increased 50 times with respect to unpatterned devices.

Keywords: Terahertz quantum cascade lasers, semiconductor microdisk lasers, vertical emission.

1. Introduction

Terahertz quantum cascade lasers (THz QCLs) were first demonstrated in 2002 [1] and have since undergone rapid development [2]. One of the most active directions of research has been the development of devices emitting in a single mode through the use of distributed feedback (DFB) resonators. Because the optical mode in these devices arises through a surface plasmon, it is possible to implement such resonators with periodically arranged slits in the top metallization [3-5]. However, due to the long wavelength, the patterns are defined with optical contact lithography, and therefore arbitrary structures can easily be implemented, which creates considerable freedom in the design of the resonator and makes them an ideal playground to test novel resonator concepts.
For example, disk lasers [6-8] are very compact, low-power devices, but have the disadvantage of low power out-coupling and non-directional emission. To address these drawbacks, we have modeled and implemented periodic gratings along the circumference of a THz QCL disk laser, shown in Fig. 1, in order to obtain vertical emission and at the same time improve power out-coupling, collection efficiency and mode-control.

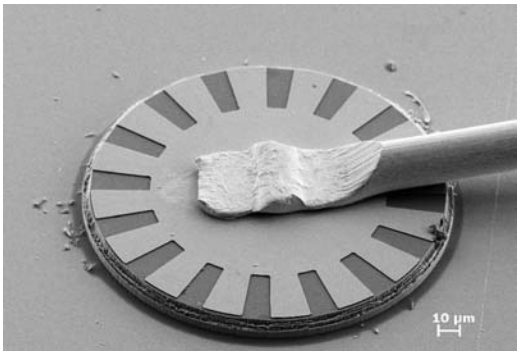

Figure 1. SEM picture of a fabricated device: The gain material is sandwiched between the bottom metal and a gear-shaped top metallization.

2. Modeling

We predict the laser oscillation in a given resonator by solving the following differential equation:

$$\left(\nabla \wedge \frac{1}{\varepsilon(\mathbf{r})} \nabla \wedge\right) \mathbf{H}(\mathbf{r}) = \frac{\omega^2}{c^2} \mathbf{H}(\mathbf{r})$$

where H is the magnetic field, ω is the angular frequency and c is the speed of light. Each domain is characterized by its complex permittivity ε, which takes into account both the relative permittivity and the loss of the material. No gain is introduced into the system (so-called cold resonator). After solving the above equation, the real part of the found eigenvalue ω gives the eigenfrequency and the imaginary part gives the inverse photon lifetime. The ratio between the two, Re(ω)/2Im(ω) gives the quality factor of the resonator. Assuming equal spatial and spectral overlap of the gain with the various resonances, laser oscillation occurs on the eigenfrequency with the highest quality factor.
A full three dimensional simulation is the easiest approach for a resonator with few symmetries, but because THz QCLs use metallic layers for mode confinement, which are typically three orders of magnitude thinner than the free-space

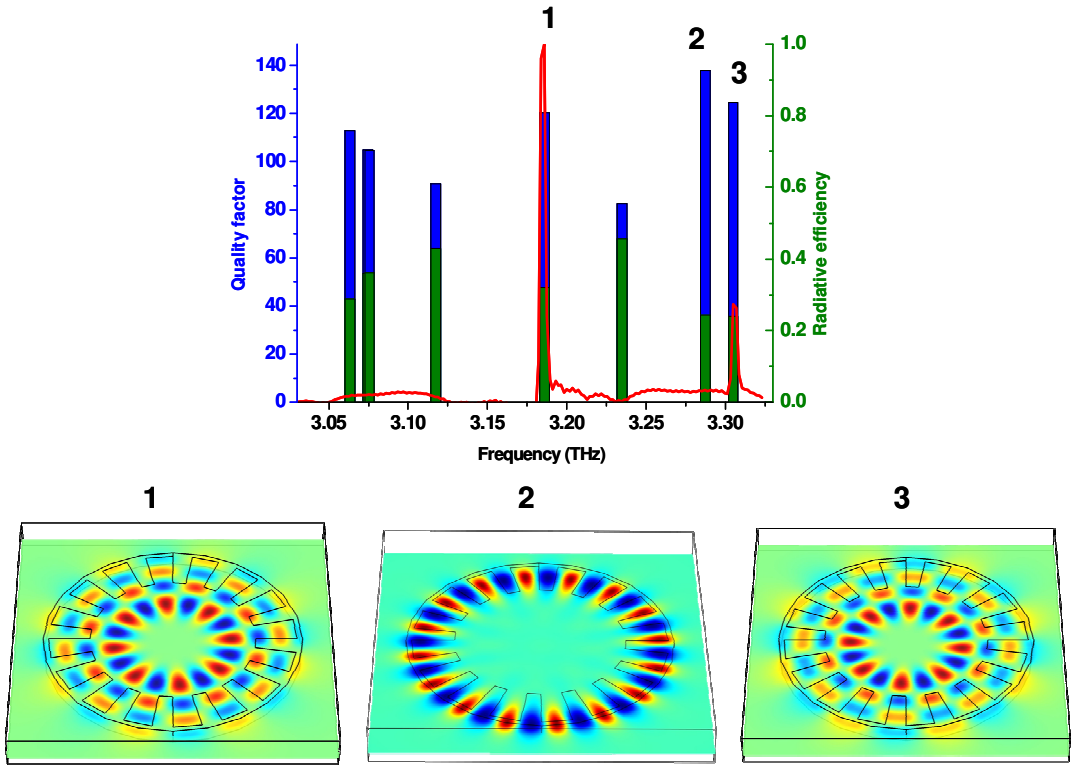

Figure 2. Computed (columns) and measured (line) spectrum of a disk with a diameter of 178 μm and 16 periods. The resonance with the highest quality factor (2) corresponds to the mode with only one radial lobe. The electric field distributions are shown in the lower panel. Due to non-uniform pumping of the disk, the observed emission frequencies instead correspond to modes with eight-fold rotational symmetry (1 and 3). Their higher radiative efficiency with respect to the mode 2 arises from the more radial nature of the mode, which in turn leads to a non-directional emission and therefore lowers collection efficiency.

wavelength, such an approach is beyond the presently available computational power. The problem is therefore solved in two steps. First we compute the complex effective refractive index of the corresponding slab waveguide using one-dimensional mode analysis. The stack consists of the GaAs/AlGaAs heterostructure sandwiched between highly doped contact layers and gold layers, which all are characterized through their refractive indices. Since the material parameters of doped semiconductors are not well known at THz frequencies, one usually relies on the approximation of the free electron gas (Drude-Lorentz). This model yields a value for the dielectric constant at a given frequency for a given doping concentration. The electron-electron scattering times are considered to be a phenomenological parameter and are taken from [9]. The optical properties of gold are taken from [10], and the refractive index of GaAs/AlGaAs heterostructure is set to 3.55, in good agreement with other devices fabricated from the same wafer. As a second step, once the effective refractive index of the slab waveguide is determined, the full three dimensional problem can be well approximated by a uniform disk with this effective refractive index, sandwiched between perfect electric conductors with the shape of the gold layers. The gear-shaped top-metallization is drawn with common drawing software and imported as a dxf-file. These simplifications allow us to perform a full 3D calculation. The whole structure is embedded in a domain of refractive index 1 with scattering boundary conditions, as shown in the lower panel of Fig. 2. In order to obtain the radiative

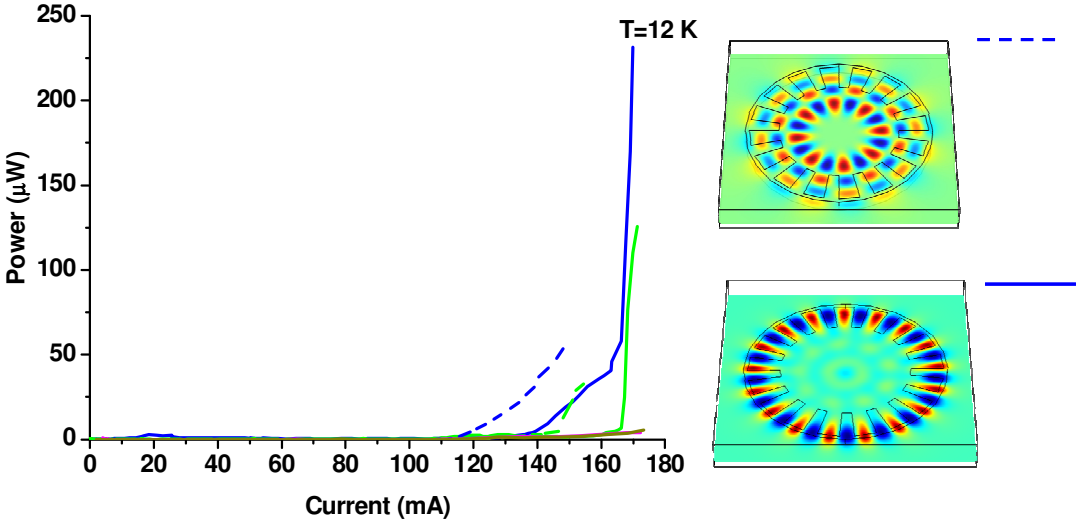

Figure 3. Solid (dashed) lines show the light-current characteristics of two devices of different diameter with 17-fold (16-fold) symmetry. For the former, very close to the maximum current, lasing occurs on the mode with only one radial lobe, with a more vertically directed emission, leading to substantially increased collection efficiency. The devices with 16-fold symmetry (dashed) lase on the mode located more in the disk centre. The colors identify devices of the same emission frequency. The lowest curves are data from disks without grating, with 50 times lower maximum power

efficiencies (out-coupling losses compared to total losses), we compute the power flow F through the transparent boundaries, normalize it with the resonator energy E, and divide it by the total losses, given by the imaginary part of the angular frequency:

$$\eta = \frac{F}{E \cdot 2 \cdot \mathrm{Im}(\omega)}$$

3. Experimental Results

We modeled disks with a diameter of about twice the free-space wavelength, or 180 μm. This corresponds to a mode with 16 azimuthal lobes along the circumference. Therefore, the top-metallization was designed as a microgear with 16 periods. Fig. 2 shows a typical eigenfrequency spectrum computed for such a device, together with the corresponding radiative efficiencies and the eigenmodes of the important resonances. A radiative efficiency around 20 % is considered a good choice for the employed gain material and waveguide. The device design supports, however, various resonances of similar quality factor, and indeed, the comparison with the measured emission plotted as a red line, shows that the device lases on two modes with eight-fold rotational symmetries. This is not surprising, because the top-metallization acts at the same time as the electrical contact, so the pumping of the mode at the circumference (mode 2 in Fig. 2) is considerably reduced. At the same time, both eight-fold modes have a well defined phase-relation with the 16-fold grating, they are just phase-shifted with respect to each other. Nevertheless, emitted power from fabricated devices is strongly increased, as shown from the dashed lines in Fig. 3, which are more than one order of magnitude above the magenta and dark-yellow line, which show the power emitted by unpatterned devices.

In order to increase the difference in quality factor between the modes, we have also modeled and fabricated devices with a grating of 17 periods. The disk size was increased by 17/16 to keep the emission frequency constant, but all the other parameters were kept unchanged. In this case, the modes equivalent to the modes 1 and 3 in Fig. 2 are still present, but no longer rotationally symmetric (no well-defined phase-relation with the grating) and have therefore a

reduced quality factor. The blue and green solid line in Fig. 3 show the measured power emitted from these devices. Very close to the maximum current, the devices lase on the mode with one radial lobe, which shows considerably higher slope efficiency. This is due to the much more vertical emission of this mode, which leads to a much higher collection efficiency with the f/1 optics we employed for the measurement.

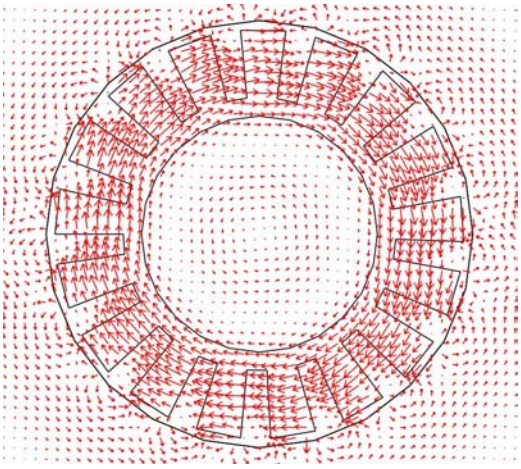

Figure 4. Computed magnetic field plotted 2 μm above the device (near-field), for the mode 2 of Fig. 2. It is dominated by an azimuthal component. Applying the Stratton-Chu formula yields the far-field shown in Fig 5.

To illustrate this further, we have exported the near-field of the vertically emitting mode (magnetic field shown in Fig. 4) and applied the Stratton-Chu formula to it, in order to obtain the far-field (see RF Module User's Guide). Since the far-field calculation of an eigenmode is not directly accessible, we implemented this with a script. The result is shown in Fig. 5. The largest part of the power is emitted under an angle of less than 30° with respect to the surface normal. This is in contrast to the modes with more radial lobes (far-field not shown), which emit under a much larger angle, and whose power is therefore much more difficult to harness with standard optics. The different slope efficiencies in Fig. 3 are thus not caused by different radiative efficiencies, but rather by a higher collection efficiency of the vertically emitting modes. This could be further improved by fabricating somewhat larger disks. A closer look at the near- and far-field of Fig. 4 and 5 show that the spacing of the far-field maxima is inversely proportional to the extent of near-field, very much in reminiscence of a double-slit diffraction pattern. An analysis along these lines show that the ring of maximum intensity can be predicted by the simple formula $\sin(2\theta) = \lambda/d$, where θ is the angle with respect to the surface normal, λ is the free-space wavelength, and d is the diameter of the ring of maximum intensity of the near-field.

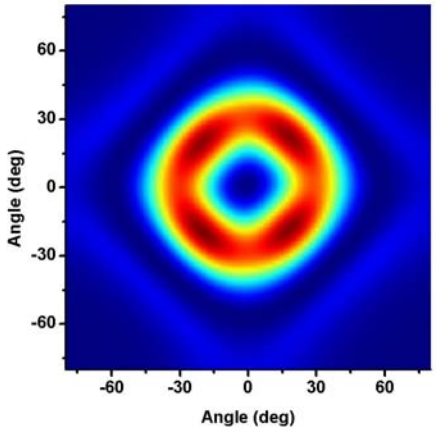

Figure 5. Computed far-field of the vertically emitting mode. The near-field, shown in Fig. 4, interferes destructively at zero angle, but still allows the collection of a significant fraction of the power with f/1 optics. A larger disk would lead to a narrower far-field.

4. Conclusions

We find a very good agreement between simulation and experiment for gratings along the perimeter of microdisk lasers fabricated from THz QCL structures. The spatial and spectral emission properties are well understood by a simplified three dimensional eigenfrequency analysis. The power collected with standard optics is experimentally shown to increase by a factor of 50.

5. References

1. R. Köhler, A. Tredicucci, F. Beltram, H. E. Beere, E. H. Linfield, A. G. Davies, D. A. Ritchie, R. C. Iotti, F. Rossi, Terahertz semiconductor-heterostructure laser, *Nature,* **417**, 156 (2002)

2. B. S. Williams, Terahertz quantum-cascade lasers, *Nature Photonics,* **1**, 517 – 525 (2007).
3. L. Mahler, A. Tredicucci, R. Köhler, H. E. Beere, E. H. Linfield, and D. A. Ritchie High-performance operation of single-mode terahertz quantum cascade lasers, *Appl. Phys. Lett.* **87**, 181101 (2005)
4. O. Demichel, L. Mahler, T. Losco, C. Mauro, R. Green, A. Tredicucci, J. Xu, F. Beltram, H. E. Beere, D. A. Ritchie, and V. Tamošinuas, Surface plasmon photonic structures in terahertz quantum cascade lasers, *Opt. Express,* **14**, 5335-5345 (2006)
5. J. A. Fan, M. A. Belkin, F. Capasso, S. Khanna, M. Lachab, A. G. Davies, and E. H. Linfield, Surface emitting terahertz quantum cascade laser with a double-metal waveguide, *Opt. Express,* **14**, 11672-11680 (2006)
6. S. L. McCall, A. F. J. Levi, R. E. Slusher, S. J. Pearton, and R. A. Logan, Whispering-gallery mode microdisk lasers, *Appl. Phys. Lett.* **60**, 289 (1992)
7. A. F. J. Levi, R. E. Slusher, S. L. McCall, J. L. Glass, S. J. Pearton, and R. A. Logan, Directional light coupling from microdisk lasers, *Appl. Phys. Lett.* **62**, 561 (1993)
8. L. A. Dunbar, R. Houdré, G. Scalari, L. Sirigu, M. Giovannini, and J. Faist, Small optical volume terahertz emitting microdisk quantum cascade lasers, *Appl. Phys. Lett.* **90**, 141114 (2007)
9. B. A. Sanborn, Electron-electron interactions, coupled plasmon-phonon modes, and mobility in n-type GaAs, *Phys. Rev. B,* **51**, 14256 (1995)
10. M. A. Ordal, R. J. Bell, R. W. Alexander, L. L. Long, M. R. Querry, Optical proprties of Au, Ni, and Pb at submilimeter wavelengths, *Applied Optics,* **26**, 744 (1987)

6. Acknowledgements

We acknowledge H.E. Beere and D.A. Ritchie, Cambridge University, for the MBE-Growth, Christoph Walther, ETH Zürich, for the waferbonding, and Bernd Witzigmann, ETH Zürich, for useful discussions.